

Article

# Enhancing the Performance of Motive Power Lead-Acid Batteries by High Surface Area Carbon Black Additives

Hai-Yan Hu <sup>1</sup>, Ning Xie <sup>2</sup>, Chen Wang <sup>1</sup>, Fan Wu <sup>1</sup>, Ming Pan <sup>1</sup>, Hua-Fei Li <sup>2</sup>, Ping Wu <sup>1</sup>, Xiao-Di Wang <sup>1</sup>, Zheling Zeng <sup>1</sup>, Shuguang Deng <sup>1,3</sup>, Marvin H. Wu <sup>4</sup>, K. Vinodgopal <sup>5,\*</sup> and Gui-Ping Dai <sup>1,\*</sup> 

<sup>1</sup> Key Laboratory of Poyang Lake Environment and Resource Utilization, Ministry of Education, School of Environmental and Chemical Engineering, Nanchang University, Nanchang 330031, Jiangxi, China; hyhu@email.ncu.edu.cn (H.-Y.H.); ncumike@163.com (C.W.); a1045344165@163.com (F.W.); mpan@email.ncu.edu.cn (M.P.); 17779606280@163.com (P.W.); 402531318006@email.ncu.edu.cn (X.-D.W.); zlzengjx@163.com (Z.Z.); shuguang.deng@asu.edu (S.D.)

<sup>2</sup> Institute for Advanced Study, Nanchang University, Nanchang 330031, Jiangxi, China; nxie@email.ncu.edu.cn (N.X.); hfli@email.ncu.edu.cn (H.-F.L.)

<sup>3</sup> School for Engineering of Matter, Transport and Energy, Arizona State University, Tempe, AZ 85287, USA

<sup>4</sup> Department of Physics, North Carolina Central University, Durham, NC 27707, USA; mwu@ncu.edu

<sup>5</sup> Department of Chemistry and Biochemistry, North Carolina Central University, Durham, NC 27707, USA

\* Correspondence: kvinodg@ncu.edu (K.V.); nanodai@gmail.com or gpdai@ncu.edu.cn (G.-P.D.)

Received: 7 December 2018; Accepted: 26 December 2018; Published: 7 January 2019



**Abstract:** The effects of carbon black specific surface area and morphology were investigated by characterizing four different carbon black additives and then evaluating the effect of adding them to the negative electrode of valve-regulated lead–acid batteries for electric bikes. Low-temperature performance, larger current discharge performance, charge acceptance, cycle life and water loss of the batteries with carbon black were studied. The results show that the addition of high-performance carbon black to the negative plate of lead–acid batteries has an important effect on the cycle performance at 100% depth-of-discharge conditions and the cycle life is 86.9% longer than that of the control batteries. The excellent performance of the batteries can be attributed to the high surface area carbon black effectively inhibiting the sulfation of the negative plate surface and improving the charge acceptance of the batteries.

**Keywords:** carbon black; nano-structure; valve-regulated lead–acid batteries; electric bikes; cycle life

## 1. Introduction

The lead–acid battery has a history of over 150 years and has a dominant position in electrochemical power supplies due to its low price, easy availability of raw materials and its full reliability in use, which is suitable for a wide range of environmental temperatures [1–5]. In the past decade, the electric bike industry has been unprecedentedly prosperous and electric bikes (e-bikes) have been gaining increasing attention in China [6]. In 2017, the total output of e-bikes in China was 29.96 million and the social ownership of e-bikes reached 250 million. However, poor cycle performance restricts the service life of valve-regulated lead–acid (VRLA) batteries for e-bikes. The e-bike batteries operate in the deep cycle duty and experience short charge and discharge pulses with high currents. The irreversible lead sulfate crystals grow on the negative electrode and form a barrier layer on the surface of the electrode, which further impedes electrolyte transfer and the charging and discharging process of the battery [7–11].

To suppress the sulfation phenomenon of the negative plate, many researchers have found that different carbon materials (such as graphite [12–15], carbon black [7,16,17], activated carbon [12,15], or graphene [18–20]) can be added to the negative active material (NAM). The addition of the carbon material can increase the specific surface area (SSA) and overall conductivity of the NAM [21,22], promote the uniform spread of the lead sulfate on the surface of the negative plate, store excess charge and build a conductive network between the lead sulfate particles [8,20].

The carbon material can effectively extend the cycle life of the battery by suppressing the growth of lead sulfate in negative plates, but the effect of extending the service life differs according to their SSA. Fernandez et al. [15] reported that the SSA of the carbon material to the NAM is an important factor that affects the electrochemical performance of negative plates. Moseley [23] found that carbon black with a higher SSA at a high-rate partial-state-of-charge (HRPSoC) was more conducive to prolonging the cycle life of hybrid electric vehicle (HEV) batteries than carbon black with a lower SSA. Zou et al. [7] pointed out that under HRPSoC conditions, the addition of 0.5 wt % carbon black to the NAM of HEV batteries increased the utilization of the active material and thus boosted the cycle life by more than 255.5% at 1 C rate discharge. Nakamura et al. [24] reported that adding a certain amount of carbon black to the NAM of HEV batteries operating in partial-state-of-charge (PSoC) conditions effectively suppressed the accumulation of  $\text{PbSO}_4$  and improved the cycle life performance due to the conductive network of carbon particles formed on the  $\text{PbSO}_4$  particles. However, most studies have added carbon black to the negative plate for VRLA batteries in HEV applications [7,23,24]. Therefore, it is quite advantageous to add high performance carbon black in the NAM to further improve the charge acceptance and deep-cycling performance of batteries for e-bike applications.

In the present work, we report, that high performance carbon black as a negative additive can significantly increase the performance of e-bike VRLA batteries. When the batteries are cycled at a  $C_2$  rate discharge under a 100% depth-of-discharge (100% DoD) condition, the cycle life of the batteries with a higher SSA of carbon black is prolonged by more than 86.9% compared to that of the control batteries with acetylene black. Moreover, both the charge acceptance and larger current discharge performance of carbon black as a negative electrode additive are improved.

## 2. Experimental Methods

### 2.1. Carbon Black Materials

In this experiment, three types of carbon black (provided by Cabot Company, Boston, MA, USA) were added to the negative plates. We studied the influence of three different SSAs of carbon black on the battery performance. Table 1 summarizes the basic physical characteristics of the three kinds of carbon black additives.

**Table 1.** Characteristics of the carbon black additives used in this work. BET = Brunauer–Emmett–Teller method.

Symbol	Negative Plate Additives	BET Surface ( $\text{m}^2 \text{g}^{-1}$ ) of Additives	Average Particle Size (nm) of Additives
Control batteries	Acetylene black	20	45.0
CB1 batteries	Carbon black 1	156	38.5
CB2 batteries	Carbon black 2	234	25.6
CB3 batteries	Carbon black 3	1378	4.3

### 2.2. Formation of VRLA Batteries

E-bike batteries (48 V/12 Ah) (Figure 1) used in this study contain four 12 V modules interconnected in series to achieve 48 volts when the amp-hour capacity (12 Ah) remains the same. Each module (Figure 1b) consists of six 2-volt cells in series and each cell was prepared with four positive and five negative plates. Between each positive and negative plate was an absorbent glass

mat (AGM) separator. The negative plate was generally obtained by using carbon black or acetylene black (control battery) additives. Based on the weight of the leady oxide powder (the oxidation degree of the leady oxide was around 76%), the carbon black and acetylene black additive content of the the NAM was 0.25 wt %. Meanwhile, with the exception of the various carbon blacks added, all conditions were exactly the same as that of a regular commercial manufacturing process of e-bike VRLA batteries. Manufacturing procedures included lead oxide power manufacturing, casting grids, slurry mixing and coating, plate curing and drying, formation of positive and negative electrodes, assembly of batteries, casting and welding, leak testing and acid (gel) filling.

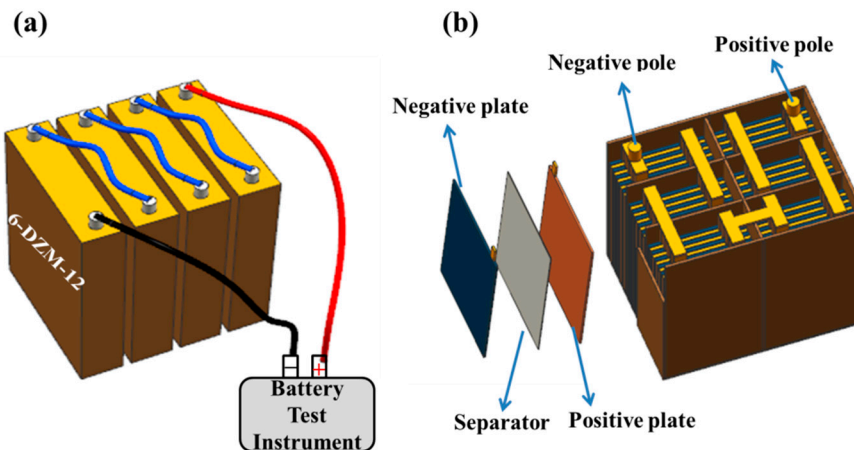


**Figure 1.** (a) Group valve-regulated lead–acid (VRLA) (48 V 12 Ah) batteries contain four 12 V 12 Ah modules and (b) schematic illustration showing a module consists of six 2-volt cells in series.

### 2.3. Battery Tests following China's Standard e-Bike Test Profile

#### 2.3.1. Capacity Test

Before a test can be performed, all test batteries need to be filled with charge. The fully charged batteries need to be cooled for 4 h to room temperature before testing.

##### Two-Hour Capacity Test

The 2-h rate capacity test includes the following process: (i) the test batteries were placed in a constant temperature box of about 25 °C for 12 h. When the temperature of the batteries reached 25 °C, the 2-h discharge capacity test was conducted; (ii) the batteries were discharged at a constant current of 6 A until the voltage decreased to 42 V and then the batteries were continuously recycled 3 times, recording the third discharge time.

##### Low-Temperature Capacity Performance Tests (−10 °C and −15 °C)

There are two research methods for low-temperature performance: one is charging at 25 °C and discharging at −15 °C. The fully charged batteries were placed in a −15 °C cold box for 12 h and then discharged at a 6 A fixed current to 42 V and the measured discharge time was recorded. After being discharged, the batteries need to be fully charged when they return to ambient temperature. The other research method involves charging and discharging at −10 °C for the whole test process. The batteries were placed in an environment at −10 °C for 12 h and then the batteries were fully charged. After, the batteries were discharged to 42 V at a fixed current of 6 A in a low temperature chamber. The whole process was repeated five times and the duration of the fifth discharge was recorded.

##### Larger Current Discharge (1.8 C<sub>2</sub>)

Batteries were placed in a temperature box of 25 °C for 4 h, then discharged to 42 V with a 1.8 C<sub>2</sub> rate and the discharge time was recorded.

### 2.3.2. Charge Acceptance

The fully charged batteries were discharged at a current of  $I_0$  ( $I_0 = C_a/10$  A, where  $C_a$  (Ah) is the maximum value in the 2 h capacity test) for 5 h under ambient temperature conditions. Immediately after discharge, the batteries were placed in a 0 °C low temperature cabinet over 20 h. Then, the batteries were removed and charged at a 57.6 V constant voltage for 10 min and the current  $I_{ca}$  was recorded. The charge acceptance ratio is  $I_{ca}/I_2$  ( $I_2 = C_2/10$  A, where  $C_2$  is the rated capacity of 2 h).

### 2.3.3. Cycling Performance Test under 100% DoD Condition

The charge and discharge cycle processes of the test batteries were carried out as follows: (i) the fully charged batteries were discharged at a 6 A ( $C_2$  rate) constant current until the voltage decreased to 42 V at ambient temperature of about 25 °C; (ii) the batteries were charged at a constant current of 2.5 A to terminal voltage of 58.8 V, then they were charged at a 58.8 V constant voltage until the final current of 0.5 A was reached before being rested for 10 min; (iii) the batteries continued charging with 55.2 V constant voltage for 4 h and then rested for 1 h; (iv) lastly, the batteries were exposed to the above charge/discharge cycle procedures until the two consecutive discharge times were below 93 min and the cycle life test was stopped.

## 2.4. Structural Characterization

The  $N_2$  adsorption/desorption isotherm and pore size distribution of carbon black additives were measured by using a Micromeritics ASAP 2460 instrument. The SSAs and pore volumes of the samples were acquired from the Brunauer–Emmett–Teller (BET) method. Pore size distribution was derived from the adsorption branch of the isotherms using the Barrett-Joyner-Halenda (BJH) model. Raman spectra of the samples were observed by a Lab RAM HR Evolution instrument using a 473 nm (blue) laser excitation. The FEI QUANTA 200F Scanning Electron Microscope (SEM) and the JEOL JEM-2100 Transmission Electron Microscope (TEM) were used to visualize the morphologies and microstructures of carbon black.

## 3. Results and Discussion

### 3.1. Morphology and Structure of Carbon Black Additives

To derive the effect of different SSA carbon blacks on the performance of VRLA batteries, three kinds of carbon black materials were characterized by different physical properties (such as BET surface area, Raman, SEM and TEM).

The SSA and pore volume of the carbon black additives were analyzed by using  $N_2$  adsorption/desorption isotherms, as shown in Figure 2a. The isotherms of carbon black samples exhibit typical IV isotherms (The IV isotherm shows a significant inflection point in the lower region of the relative pressure ( $P/P_0$ ), and hysteresis loops occur under higher pressure due to the phenomenon of capillary condensation.) with a significant hysteresis loop, indicating the presence of a typical mesoporous structure in all samples [25]. The BET surface areas of carbon black 1 (CB1), CB2 and CB3 were  $156 \text{ m}^2 \text{ g}^{-1}$ ,  $234 \text{ m}^2 \text{ g}^{-1}$  and  $1378 \text{ m}^2 \text{ g}^{-1}$ , with BJH adsorption cumulative volumes of pores of  $0.387 \text{ cm}^3 \text{ g}^{-1}$ ,  $1.100 \text{ cm}^3 \text{ g}^{-1}$  and  $1.129 \text{ cm}^3 \text{ g}^{-1}$ , respectively. It is apparent that the CB3 sample possesses a larger surface area and a higher pore volume. Figure 2b shows the pore size distribution of the three carbon black samples. There is only one mesopore peak in the curve of CB1 and CB3, which is mainly centered at 2.5 nm and 10 nm, respectively. However, the CB2 sample has two pore-size distribution peaks and the peaks of mesopore and macropore were about 2.5 nm and 50 nm, respectively. Carbon black with suitable mesopore distribution facilitates rapid diffusion of the acid electrolyte and promotes ion diffusion during the electrochemical processes [26]. Therefore, the mesoporous structure is conducive to improving the charge acceptance of VRLA batteries for e-bikes in the deep cycle duty.

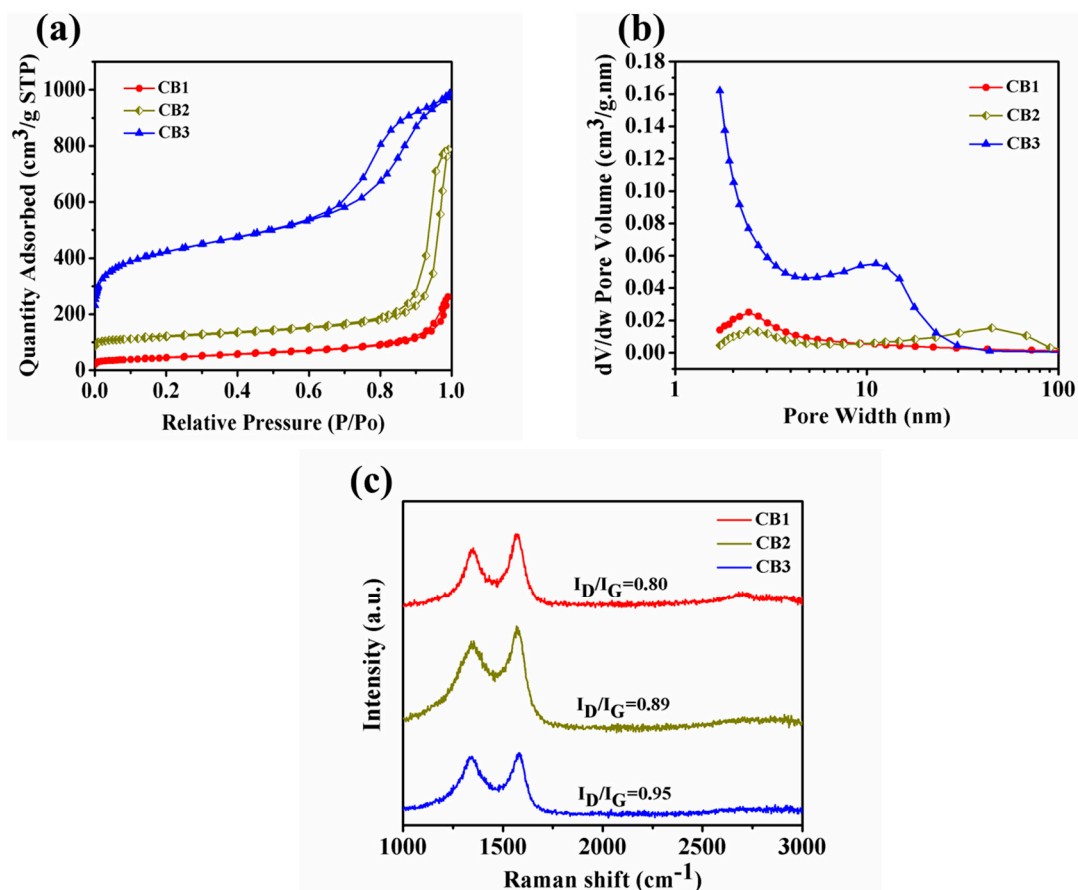


**Figure 2.** (a) Nitrogen adsorption/desorption isotherms at standard temperature and pressure (STP), (b) Barrett-Joyner-Halenda (BJH) model pore size distribution,  $dV/dw$  refers to the change rate of pore volume with pore size. (c) Raman spectra of carbon black 1 (CB1), CB2 and CB3,  $I_D/I_G$  is the ratio of the intensity of D peak to that of G peak.

As seen in Figure 2c, the Raman spectra of carbon black exhibits two main characteristic peaks: the D band ( $1350\text{ cm}^{-1}$ ) is known as the disordered band and is caused by defects in the lattice of carbon atom, and the G band ( $1568\text{ cm}^{-1}$ ) reflects the crystalline and graphitic structure of the carbon materials [27]. The structural defects and the indication of disorder of the carbon black material can be characterized by the intensity ratio of  $I_D/I_G$  [28].  $I_D/I_G$  is the ratio of the intensity of the D peak to that of the G peak. This ratio generally indicates the degree of defect density of the carbon material, and the larger the ratio of  $I_D/I_G$ , the greater the degree of defect of the material. Therefore, in the Raman spectra, the  $I_D/I_G$  values of CB1, CB2 and CB3 are calculated to be 0.80, 0.89 and 0.95, respectively, indicating that the CB3 sample has more defective sites. Accordingly, with the increase of SSA and pore volume, the defect degree of the samples is also increased. Meanwhile, the ratio of  $I_D/I_G$  is inversely proportional to the grain size, which is confirmed by TEM observations.

The morphology and microstructure of three samples with different SSAs of carbon black is studied by SEM, TEM and high-resolution TEM (HRTEM), as shown in Figure 3. From the SEM images, it can be seen that the CB1 (Figure 3a), CB2 (Figure 3b) and CB3 (Figure 3c) particles have a spherical structure. The mean size of CB1 particles is about 38 nm and they exhibited a certain degree of agglomeration. The average particle size of CB3 (about 4 nm) is significantly smaller than that of CB2 (about 25 nm) and the aggregation of the small particles of CB3 is more severe than CB2. Furthermore, the CB1 particle size is obviously larger than that of the other two particles. As the particle size decreases, the SSA of carbon black increases. Figure 3d–g further verify that CB1, CB2 and CB3 particles are irregular spherical structures whose particle size is basically consistent with the structure range obtained from the SEM images. At the same time, it can be seen by the HRTEM

(Figure 3h–j) images that the graphite layer inside the carbon black is randomly arranged, showing disorder phenomenon, indicating that carbon black is an amorphous structure. The carbon black particles are connected to each other to form a network structure and the presence of pore structures in these network structures is mainly derived from unfilled voids between the particles. The pore structure of carbon black provides channels for the transmission of the acid electrolyte and facilitates the full contact between the electrolyte and the surface of the negative material.

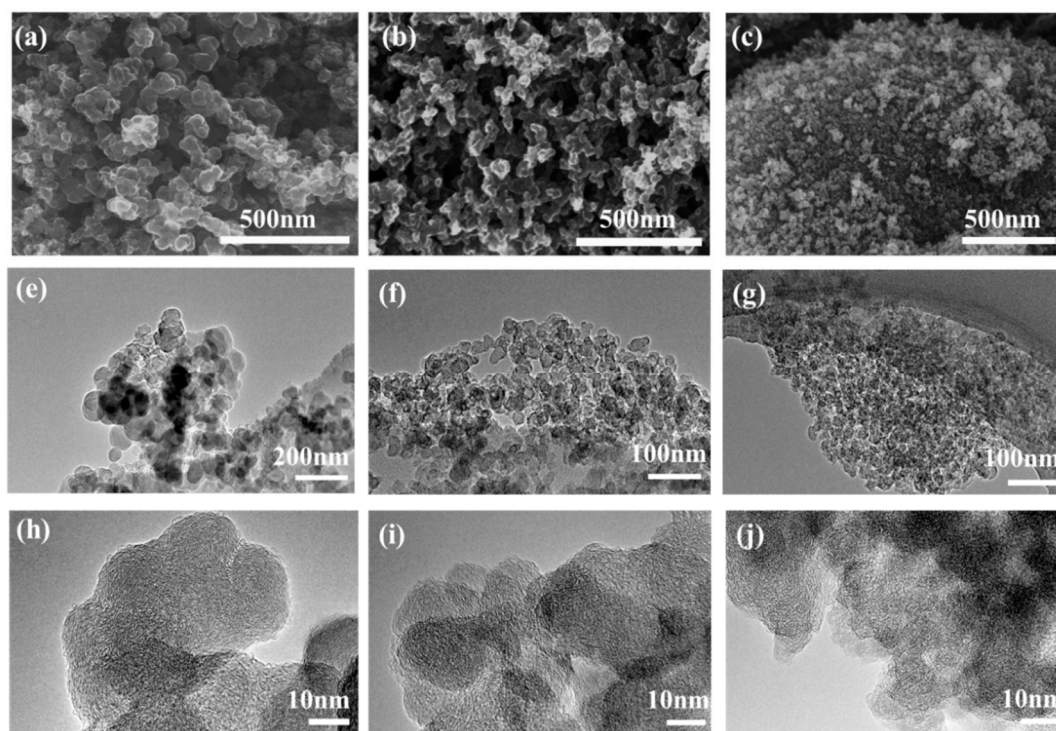


**Figure 3.** (a–c) Scanning electron microscopy (SEM) images, (e–g) transmission electron microscopy (TEM) images, (h–j) high-resolution TEM (HRTEM) images of CB1, CB2 and CB3, respectively.

### 3.2. Performance Tests of VRLA Batteries

#### 3.2.1. Discharge Capacity Tests

As shown in Figure 4, VRLA batteries with different carbon black materials at 2-h rate, low-temperature performance and 1.8 C<sub>2</sub> discharge performance were compared to those of the control batteries with acetylene black as a negative electrode additive.

Figure 4a shows the 2-h rate capacity test of VRLA batteries. As can be seen in the figure, the discharge times of CB1, CB2, CB3 and the control batteries at room temperature are 126 min, 127 min, 128 min and 125 min, respectively. When CB3 is added as a negative electrode additive, the discharge capacity of the batteries is highest and the discharge time is 128 min, which is 2.4% higher than that of the control batteries. Experimental results show that with the increase of SSA of carbon black, the discharge capacity of the batteries is also increased.

A battery's low-temperature capacity is related to temperature. If the battery's discharge capacity is lower than the standard value (85 min) at low temperatures, the battery efficiency will decrease under cold conditions, especially in northern China. In this paper, there are two research methods for low-temperature performance: one is charging at 25 °C and discharging at −15 °C, and the other is charging and discharging at −10 °C. Figure 4b shows a significant improvement of the discharge time of the batteries containing carbon black at a low temperature of −15 °C. The discharge times of CB1, CB2, CB3 and the control batteries are 103 min, 105 min, 110 min and 100 min, respectively. It can be found that the discharge time of the batteries with carbon black has a marginal improvement of 3–10%

compared to the control batteries [29]. The low temperature  $-10\text{ }^{\circ}\text{C}$  performance test is shown in Figure 4c. These data indicate that batteries with carbon black additives have a significant improvement of 2–5% when compared to the control batteries. The results of the low-temperature discharge test at  $-15\text{ }^{\circ}\text{C}$  and  $-10\text{ }^{\circ}\text{C}$  indicate that carbon black as negative additives have better low-temperature performance and have a longer lifetime in low-temperature environments. In addition, CB3 has better low-temperature performance, which is due to the larger SSA of the CB3 additive, which can better improve the migration rate of ions [30].

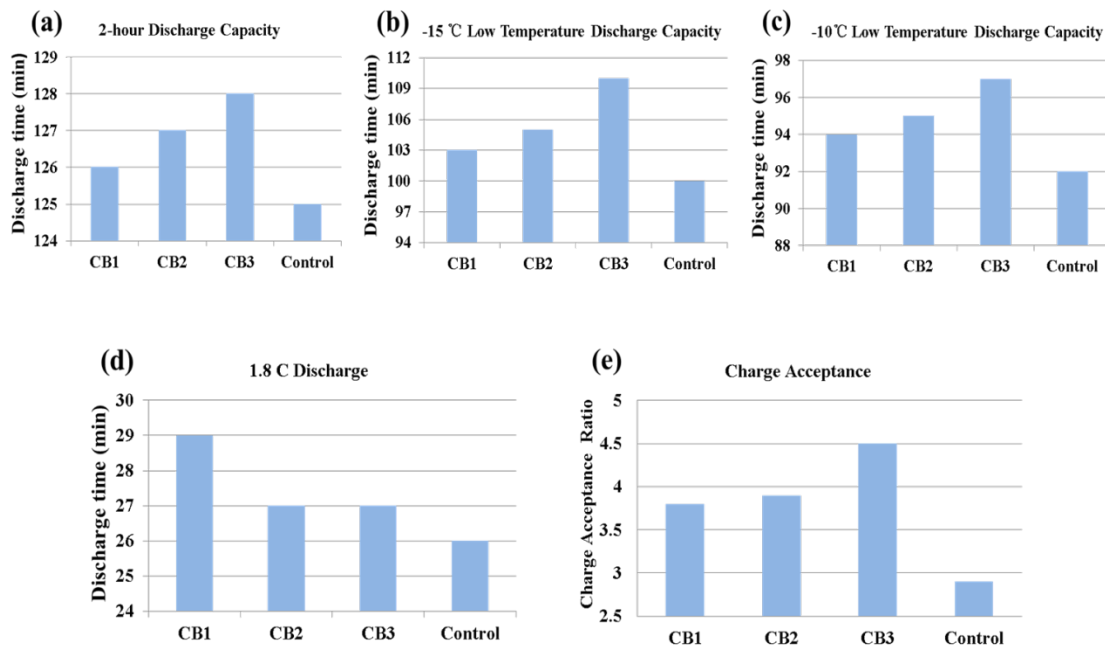


**Figure 4.** (a) Two-hour capacity tests at room temperature, (b,c) low-temperature performance tests at  $-15\text{ }^{\circ}\text{C}$  and  $-10\text{ }^{\circ}\text{C}$  of VRLA (48 V 12 Ah) batteries with carbon black additives with different SSAs, respectively. (d) Effect of carbon black on high-current discharge performance. (e) Effect of carbon black on charge acceptance performance.

E-bikes have a large current discharge when they start, which has a great impact on the life of the batteries. It is observed from Figure 4d that the discharge time of the batteries with carbon black is slightly better than the control batteries at 1.8 C<sub>2</sub> rate discharge. Compared with the C<sub>2</sub> rate discharge at 25 °C, the discharge capacity of the large current discharge is significantly decreased. This is probably because the reaction occurs only on the surface of the active material on the negative plate when a large current is discharged. PbSO<sub>4</sub> crystals form an irreversible PbSO<sub>4</sub> layer on the surface of the negative plate, which further impedes the HSO<sub>4</sub><sup>-</sup> ions into the interior of the plate and reduces the reversible electrochemical reaction, which leads to the premature reduction of the battery's capacity [31].

### 3.2.2. Charge Acceptance

The charge acceptance capability of VRLA batteries is an important performance metric for e-bike applications. It not only represents the recharge ability of the batteries, but also objectively reflects the service life of the batteries. The charge acceptance ratio ( $I_{ca}/I_2$ ) of batteries with different additives is shown in Figure 4e. A higher charge acceptance ratio demonstrates that the batteries have better charge acceptance [32]. The batteries exhibit better charge acceptance and their current acceptance is better. At the same time, the polarization of the batteries is not easy to achieve, thereby prolonging the cycle life of the batteries. The  $I_{ca}/I_2$  value of CB1, CB2, CB3 and the control batteries are 3.8, 3.9, 4.5 and 2.9, respectively. Compared with the control batteries, the increase ranges between 30% and 55% with carbon black batteries. Furthermore, the charge acceptance ratio of batteries containing

high-SSA carbon black is superior to that of those containing low-SSA carbon black. These results clearly show the strong effect of the SSA of the carbon additive. The CB3 additive has a large SSA and the particles are interconnected to form a three-dimensional (3D) network structure, which provides a larger active SSA for the crystallization and dissolution of lead sulfate particles, thus improving the charge acceptance of the batteries [32,33].

### 3.2.3. Cycling Performance

Charge and discharge cycle life is a key parameter to measure VRLA battery performance. Figure 5 shows the dependence of the discharge time of four batteries on cycle number at  $C_2$  rate discharge under 100% DoD conditions. The actual discharge capacity of the batteries was the discharge current multiplied by the discharge duration. In the initial cycle, the capacity of the batteries increased because of the activation process. The discharge capacity of the control batteries was reduced sharply during the cycle and failed after only 225 cycles. From this figure, at  $C_2$  rate discharge, the cycle numbers of the CB1, CB2 and CB3 batteries were 350, 350 and 430, respectively, which are 52.2%, 52.2% and 86.9% higher than those of the controls, respectively, indicating that the addition of carbon black to the negative plate of the batteries can extend the cycle life of the batteries. Moreover, the trend of CB1 and CB2 batteries showed no significant difference under 100% DoD test conditions. CB3 batteries have longer cycle life than CB1 and CB2 batteries, which may be due to the uneven dispersion of CB1 and CB2 particles on the plate [34]. In addition, the discharge time of the batteries with CB3 held steady during 300 charge/discharge cycles, but the discharge time decreased rapidly after 300 cycles, possibly due to the stratification of electrolytes and the excessive loss of water in the electrolytes [13,35]. As the cycle number of the battery increases, a large amount of big and dense  $PbSO_4$  particles accumulate on the surface of the negative plate so that the Ohmic resistance of the batteries continuously increases during the charge/discharge process, causing the capacity to decline prematurely and accelerating battery failure.

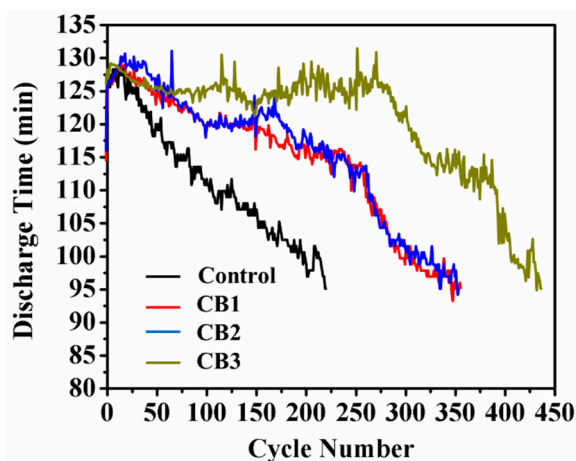


**Figure 5.** Effect of carbon black on the cycle life of VRLA (48 V/12 Ah) batteries under 100% depth-of-discharge (DoD) conditions at  $C_2$  discharge rate (6 A). Plots of the discharge time and the number of cycles for three different specific surface areas (SSAs) of carbon black are used as negative additives for lead–acid batteries and acetylene black as a control additive.

Based on the above results, it is possible to conclude that carbon black with high SSA has better performance than carbon black with low SSA when added to the negative plate, which could effectively inhibit the irreversible sulfation of VRLA batteries and prolong the cycle life [36]. In addition, the number of cycles of CB3 batteries increased by 86.9% compared to the control batteries at 100% DoD conditions. These results can be attributed to the carbon black with greater SSA than acetylene black.

### 3.2.4. Water Loss Performance

During the cycle life of VRLA batteries for e-bikes, one of the main reasons for the failure of VRLA batteries is dry failure due to lack of water. The main reason for this is that the float charge voltage is high, causing the battery to lose water faster, so that the battery cannot work normally because of the excessive polarization in the charging and discharging process. At the end of charging, the decomposition of water leads to the separation of hydrogen and oxygen; this is the main factor of water loss. The oxygen gas can perform the oxygen recombination reaction on the negative plate, while the hydrogen cannot be absorbed and can only gather at the top of the battery [1,37]. When the hydrogen gas reaches a certain amount, the safety valve automatically opens and releases gas, causing water loss. The addition of additives to the negative active material can improve the battery's charge acceptance and low temperature performance. However, the presence of some carbon additives may reduce the hydrogen evolution over-potential of the negative electrode, leading to an increase in the hydrogen evolution of the negative electrode. Carbon black as an active additive of the negative electrode has an important effect on water loss of the batteries.

The water loss of the four batteries during the cycle is shown in Figure 6. In the figure, with the increase in cycle number, the water loss of the control batteries increased from 6.5 g to 17.1 g. In addition, the water loss of the carbon black batteries increased only slightly between 200 cycles of the control batteries, indicating that the water loss of the batteries containing carbon black was within a controllable range and there was no obvious difference from the control batteries. The water loss of the batteries with carbon black reached 30.8–31.2 g after 350 cycles. Moreover, the CB3 battery water loss reached 36.1 g after 400 cycles. The water loss of the battery can increase the acid concentration, aggravate the sulfation degree of the negative plate, magnify the internal resistance, depress the battery capacity, shorten the battery service life and even lead to the thermal runaway of the battery [16,38].

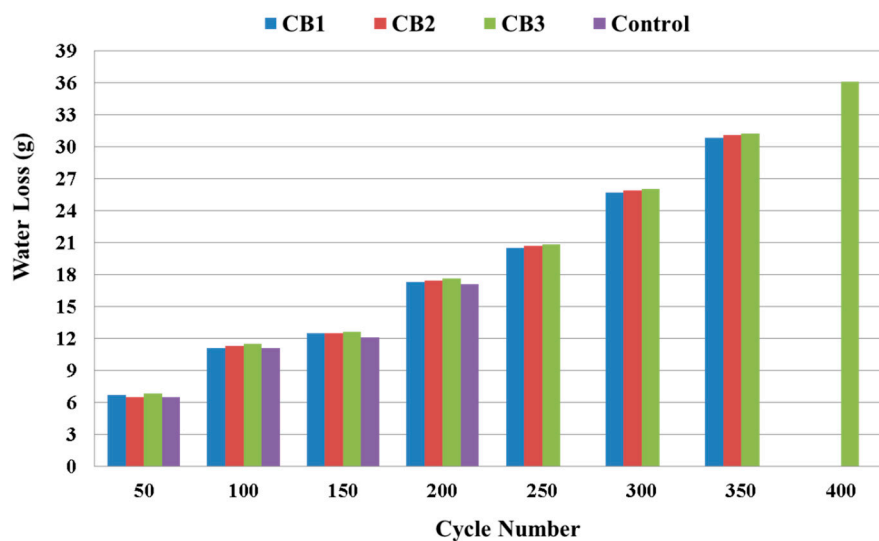
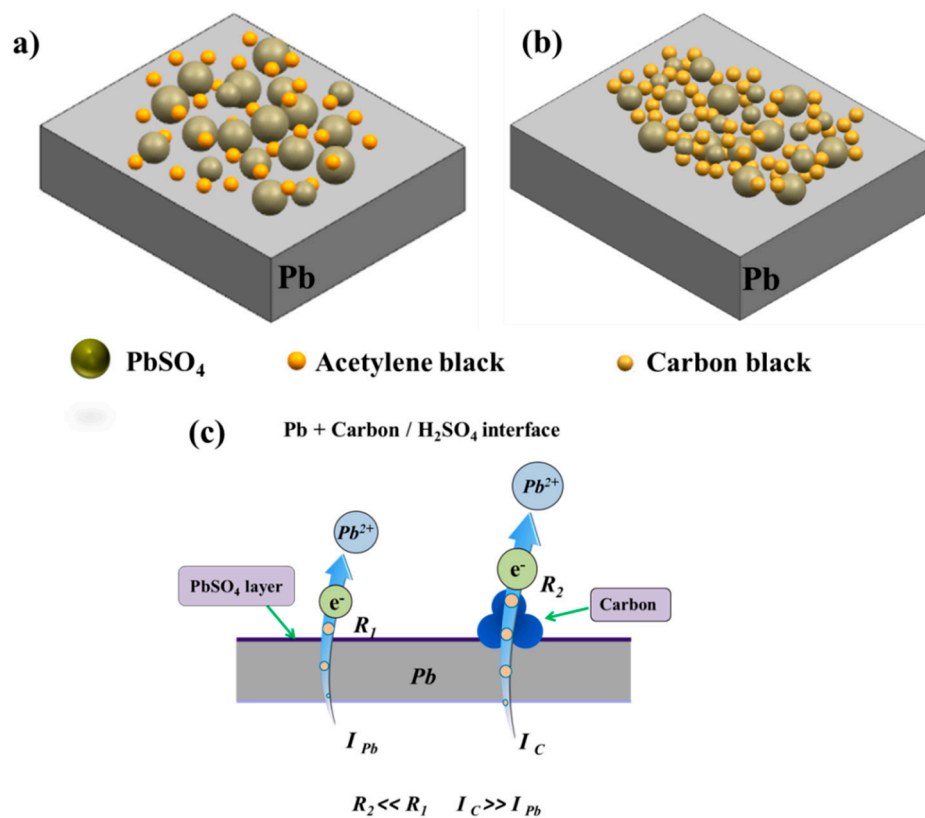


Figure 6. Diagram of the relationship between water loss and the number of cycles.

### 3.3. Mechanism of the Effect of Adding Carbon Black on the Negative Plate

Based on the above research results, a model that can extend the service life of the battery by adding carbon black is proposed. This model can better explain the surface reaction of the battery negative plate when the batteries of e-bikes are charged and discharged in deep cycle duty under 100% DoD conditions. During charging, small lead sulfate crystals with high solubility can be reduced to lead. The large  $\text{PbSO}_4$  crystals with poor solubility can hardly be reduced and recrystallized into larger lead sulfate particles on the surface of the negative plates [7,32,39]. As is well known, acetylene black and carbon black are small spherical structures. When acetylene black (Figure 7a) and carbon black (Figure 7b) are added as negative additives, point-to-point contact will be formed between

carbon particles and PbSO<sub>4</sub> particles and acetylene black particles may be independently dispersed on the negative plate to form conductive channels. For carbon black, the main factor influencing the conductive properties of carbon black is its structure, such as the degree of branching of carbon black. High-structure carbon black has a more developed chain structure than aggregates of low structural carbon black. It is possible that carbon black particles with high SSA are in contact with each other to form a continuous bead-like conductive network structure, while the low SSA carbon black forms a discontinuous chain structure due to the larger particle size. The less contact sides the carbon particles have between each other, the worse the charge transport and the electrical conductivity, so high SSA carbon black is more favorable for the diffusion of the electrolyte from the surface to the inside of the plate and the formation of small-sized lead sulfate crystals with high solubility [23,40]. Therefore, the high SSA carbon black additive can better inhibit the growth of the lead sulfate crystal on the negative plate and prolong the cycle life of the battery.



**Figure 7.** (a,b) Schematic diagram of acetylene black and carbon black on the negative plate under 100% DoD conditions, respectively. (c) Schematic diagram of ion migration through the Pb and carbon interfaces in the negative plate. ( $R_1$  and  $I_{Pb}$  are the resistance and current of ions passing through the interface of Pb/H<sub>2</sub>SO<sub>4</sub>, respectively.  $R_2$  and  $I_C$  are the resistance and current of ions passing through the interface of C/H<sub>2</sub>SO<sub>4</sub>, respectively.)

Pavlov [41] proposed a model for the parallel mechanism of charge in which the electrochemical reaction process of the lead negative electrode occurs on both the surface of Pb and carbon black particles during the cycling of batteries under 100% DoD conditions. The electron migration diagram of Pb and carbon interface in negative plates is presented in Figure 7c. With the progress of the reaction, the PbSO<sub>4</sub> crystals grow continuously to form a rough and dense irreversible PbSO<sub>4</sub> layer on the surface of Pb and the barrier layer of PbSO<sub>4</sub> not only hinders the ion migration, but also amplifies the charge transfer resistance ( $R_1$ ) at the interface of Pb/H<sub>2</sub>SO<sub>4</sub> [15,41]. However, the PbSO<sub>4</sub> barrier layer is not formed at the C/H<sub>2</sub>SO<sub>4</sub> interface because the mesopores of carbon material construct the channel of ion diffusion and migration, thus the resistance ( $R_2$ ) of ions passing through the C/H<sub>2</sub>SO<sub>4</sub> interface

is much smaller than that of  $R_1$ . Although CB1, CB2 and CB3 batteries have the same proportion of carbon black, CB3 batteries have carbon black that is evenly dispersed on the negative electrode surface compared to the other two types of batteries and its effect as an ion transport channel is greatly increased. As the particle size of CB3 is smaller than that of CB1 and CB2, it is easily dispersed well among the active material. Correspondingly, the batteries containing CB3 have excellent high-rate charge and discharge performance.

#### 4. Conclusions

In this study, carbon black with different SSAs was used as the negative electrode additive of power VRLA batteries for e-bikes. The low-temperature performance, charge acceptance, larger current discharge performance and cycle life of VRLA batteries were investigated. The results show that compared with the control batteries containing acetylene black, adding carbon black additives to the batteries can significantly enhance the low-temperature performance, improve the charge acceptance and prolong cycle life at 100% DoD conditions. The cycle life of batteries with carbon black increased from 225 to 430 times under 100% DoD conditions, which is 86.9% higher than that of the control batteries. Furthermore, the water loss of carbon black batteries was not significantly different from that of control batteries. In addition, CB3 batteries had the most stable cycle performance and more remarkable charge acceptance stability, which is due to the larger SSA and pore volume of CB3. A larger SSA enlarges the electrochemical active surface of the active material and the smaller particle size carbon black is more easily dispersed within the active material. Carbon black has a rich mesoporous structure. Adding carbon black to the negative plate can effectively construct the internal and external transmission channels of the plate, increase the migration rate of ions, effectively alleviate the generation of negative plate sulfation and improve the battery's charging acceptance performance and cycle life.

**Author Contributions:** G.-P.D. conceived and designed the experiments; H.-Y.H. performed the experiments; X.N., C.W., F.W., H.-F.L., M.P., P.W., X.D.W., Z.-L.Z., S.D., K.V., and G.-P.D. analyzed the data; M.H.W. contributed reagents/materials/analysis tools; H.-Y.H., K.V., and G.-P.D. wrote the paper.

**Funding:** This research was funded by National Natural Science Foundation of China (Grants 51462022 and 51762032) and the Natural Science Foundation Major Project of Jiangxi Province of China (Grant 20152ACB20012) and NSF PREM (Award DMR 1523617).

**Acknowledgments:** G.-P.D. acknowledges the National Natural Science Foundation of China (Grants 51462022 and 51762032) and the Natural Science Foundation Major Project of Jiangxi Province of China (Grant 20152ACB20012) for financial support of this research. K.V. and M.H.W. acknowledge the support of NSF PREM Award DMR 1523617. The assistance of Zhi-Qun Tian (HRTEM measurements) at Guangxi University and A.S. Kumbhar (SEM and HRTEM measurements), CHANL at UNC Chapel Hill, is also greatly appreciated.

**Conflicts of Interest:** The authors declare no conflicts of interest.

#### References

1. Yang, J.; Hu, C.; Wang, H.; Yang, K.; Liu, J.B. Review on the research of failure modes and mechanism for lead-acid batteries: Reviews on the research of failure modes for lead-acid batteries. *Int. J. Energy Res.* **2017**, *41*, 336–352. [[CrossRef](#)]
2. Lam, L.T.; Newnham, R.H.; Ozgun, H.; Fleming, F.A. Advanced design of valve-regulated lead-acid battery for hybrid electric vehicles. *J. Power Sources* **2000**, *88*, 92–97. [[CrossRef](#)]
3. Zheng, S.; Jia, G.; Xue, W.; Huang, B. Performance of a lead-carbon negative electrode based on a Pb-C electrodeposited porous graphite/Pb conductive net skeleton. *Micro Nano Lett.* **2016**, *11*, 264–268. [[CrossRef](#)]
4. Huang, T.; Ou, W.; Feng, B.; Huang, B.; Liu, M.; Zhao, W.; Guo, Y. Researches on current distribution and plate conductivity of valve-regulated lead-acid batteries. *J. Power Sources* **2012**, *210*, 7–14. [[CrossRef](#)]
5. Enos, D.G.; Ferreira, S.R.; Barkholtz, H.M.; Baca, W.; Fenstermacher, S. Understanding Function and Performance of Carbon Additives in Lead-Acid Batteries. *J. Electrochem. Soc.* **2017**, *164*, A3276–A3284. [[CrossRef](#)]

6. Muetze, A.; Tan, Y.C. Electric bicycles—A performance evaluation. *Ind. Appl. Mag. IEEE* **2007**, *13*, 12–21. [[CrossRef](#)]
7. Zou, X.; Kang, Z.; Dong, S.; Liao, Y.; Gong, Y.; He, C.; Hao, J.; Zhong, Y. Effects of carbon additives on the performance of negative electrode of lead-carbon battery. *Electrochim. Acta* **2015**, *151*, 89–98. [[CrossRef](#)]
8. Pavlov, D.; Nikolov, P.; Rogachev, T. Influence of carbons on the structure of the negative active material of lead-acid batteries and on battery performance. *J. Power Sources* **2011**, *196*, 5155–5167. [[CrossRef](#)]
9. Marom, R.; Ziv, B.; Banerjee, A.; Cahana, B.; Luski, S.; Aurbach, D. Enhanced performance of starter lighting ignition type lead-acid batteries with carbon nanotubes as an additive to the active mass. *J. Power Sources* **2015**, *296*, 78–85. [[CrossRef](#)]
10. Guo, Y.; Tang, S.; Meng, G.; Yang, S. Failure modes of valve-regulated lead-acid batteries for electric bicycle applications in deep discharge. *J. Power Sources* **2009**, *191*, 127–133. [[CrossRef](#)]
11. Lam, L.T.; Haigh, N.P.; Phyland, C.G.; Urban, A.J. Failure mode of valve-regulated lead-acid batteries under high-rate partial-state-of-charge operation. *J. Power Sources* **2004**, *133*, 126–134. [[CrossRef](#)]
12. Wang, L.Z.; Zhang, K.Q.; Zhang, L.S.; Zhang, Y.; Wang, K. Effect of carbon materials on electrochemical characteristics of negative electrodes of lead-acid battery. *Chin. J. Power Sources* **2012**, *9*, 22. [[CrossRef](#)]
13. Valenciano, J.; Sánchez, A.; Trinidad, F.; Hollenkamp, A.F. Graphite and fiberglass additives for improving high-rate partial-state-of-charge cycle life of valve-regulated lead-acid batteries. *J. Power Sources* **2006**, *158*, 851–863. [[CrossRef](#)]
14. Jaiswal, A.; Chalasani, S.C. The role of carbon in the negative plate of the lead-acid battery. *J. Energy Storage* **2015**, *1*, 15–21. [[CrossRef](#)]
15. Fernández, M.; Valenciano, J.; Trinidad, F.; Muñoz, N. The use of activated carbon and graphite for the development of lead-acid batteries for hybrid vehicle applications. *J. Power Sources* **2010**, *195*, 4458–4469. [[CrossRef](#)]
16. Pavlov, D.; Nikolov, P. Capacitive carbon and electrochemical lead electrode systems at the negative plates of lead-acid batteries and elementary processes on cycling. *J. Power Sources* **2013**, *242*, 380–399. [[CrossRef](#)]
17. Atanassova, P.; Bliznac, B.; Koehlert, K.C.; Moeser, G.D.; Oljaca, M.; Sun, Y.; Pierre, D.; Sawrey, J.S. Carbon Blacks and Use in Electrodes for Lead Acid Batteries. U.S. Patent 9,287,565[p], 15 March 2016.
18. Yeung, K.K.; Zhang, X.; Ciucci, F.; Yuen, M.M.F. Enhanced Cycle Life of a Lead-acid Battery Using Graphene as a Sulfation Suppression Additive in Negative Plates. *RSC Adv.* **2015**, *5*, 71314–71321. [[CrossRef](#)]
19. Li, X.; Zhang, Y.; Su, Z.; Zhao, Y.; Zhao, X.; Wang, R. Graphene nanosheets as backbones to build a 3D conductive network for negative active materials of lead-acid batteries. *J. Appl. Electrochem.* **2017**, *47*, 1–12. [[CrossRef](#)]
20. Long, Q.; Ma, G.; Xu, Q.; Ma, C.; Nan, J.; Li, A.; Chen, H. Improving the cycle life of lead-acid batteries using three-dimensional reduced graphene oxide under the high-rate partial-state-of-charge condition. *J. Power Sources* **2017**, *343*, 188–196. [[CrossRef](#)]
21. Nakamura, K.; Shiomi, M.; Takahashi, K.; Tsubota, M. Failure modes of valve-regulated lead/acid batteries. *J. Power Sources* **1996**, *59*, 153–157. [[CrossRef](#)]
22. Moseley, P.T.; Nelson, R.F.; Hollenkamp, A.F. The role of carbon in valve-regulated lead-acid battery technology. *J. Power Sources* **2006**, *157*, 3–10. [[CrossRef](#)]
23. Moseley, P.T. Consequences of including carbon in the negative plates of Valve-regulated Lead-Acid batteries exposed to high-rate partial-state-of-charge operation. *J. Power Sources* **2009**, *191*, 134–138. [[CrossRef](#)]
24. Shiomi, M.; Funato, T.; Nakamura, K.; Takahashi, K.; Tsubota, M. Effects of carbon in negative plates on cycle-life performance of valve-regulated lead-acid batteries. *J. Power Sources* **1997**, *64*, 147–152. [[CrossRef](#)]
25. Qin, C.; Ji, L.; Wu, K.; Zhang, W. Morphology-dependent Electrochemical Enhancements of Porous Carbon as Sensitive Determination Platform for Ascorbic Acid, Dopamine and Uric Acid. *Sci Rep.* **2016**, *6*, 22309.
26. Gai, Y.; Shang, Y.; Gong, L.; Su, L.; Hao, L.; Dong, F.; Li, J. A self-template synthesis of porous ZnCo<sub>2</sub>O<sub>4</sub> microspheres for high-performance quasi-solid-state asymmetric supercapacitors. *RSC Adv.* **2017**, *7*, 1038–1044. [[CrossRef](#)]
27. Xia, J.; Zhang, L.; Fu, Y.; He, G.; Sun, X.; Wang, X. Nitrogen-doped carbon black supported NiCo<sub>2</sub>S<sub>4</sub> catalyst for hydrogenation of nitrophenols under mild conditions. *J. Mater. Sci.* **2018**, *53*, 4467–4481. [[CrossRef](#)]
28. Gurunathan, S.; Han, J.W.; Kim, J.H. Green chemistry approach for the synthesis of biocompatible graphene. *Int. J. Nanomed.* **2013**, *8*, 2719–2732. [[CrossRef](#)]

29. Swogger, S.W.; Everill, P.; Dubey, D.P.; Sugumaran, N. Discrete carbon nanotubes increase lead acid battery charge acceptance and performance. *J. Power Sources* **2014**, *261*, 55–63. [[CrossRef](#)]
30. Hong, B.; Jiang, L.; Xue, H.; Liu, F.; Jia, M.; Li, J.; Liu, Y. Characterization of nano-lead-doped active carbon and its application in lead-acid battery. *J. Power Sources* **2014**, *270*, 332–341. [[CrossRef](#)]
31. Lam, L.T.; Haigh, N.P.; Phyland, C.G.; Huynh, T.D. Novel technique to ensure battery reliability in 42-V PowerNets for new-generation automobiles. *J. Power Sources* **2005**, *144*, 552–559. [[CrossRef](#)]
32. Xiang, J.; Ding, P.; Zhang, H.; Wu, X.; Chen, J.; Yang, Y. Beneficial effects of activated carbon additives on the performance of negative lead-acid battery electrode for high-rate partial-state-of-charge operation. *J. Power Sources* **2013**, *241*, 150–158. [[CrossRef](#)]
33. Blecua, M.; Fatas, E.; Ocon, P.; Gonzalo, B.; Merino, C.; Fuente, F.D.L.; Valenciano, J.; Trinidad, F. Graphitized Carbon Nanofibers: New additive for the Negative Active Material of Lead Acid Batteries. *Electrochim. Acta* **2017**, *257*, 109–117. [[CrossRef](#)]
34. Ebner, E.; Burow, D.; Panke, J.; Börger, A.; Feldhoff, A.; Atanassova, P.; Valenciano, J.; Wark, M.; Rühl, E. Carbon blacks for lead-acid batteries in micro-hybrid applications—Studied by transmission electron microscopy and Raman spectroscopy. *J. Power Sources* **2013**, *222*, 554–560. [[CrossRef](#)]
35. Tantichanakul, T.; Chailapakul, O.; Tantavichet, N. Gelled electrolytes for use in absorptive glass mat valve-regulated lead-acid (AGM VRLA) batteries working under 100% depth of discharge conditions. *J. Power Sources* **2011**, *196*, 8764–8772. [[CrossRef](#)]
36. Wang, L.; Zhang, H.; Cao, G.; Zhang, W.; Zhao, H.; Yang, Y. Effect of activated carbon surface functional groups on nano-lead electrodeposition and hydrogen evolution and its applications in lead-carbon batteries. *Electrochim. Acta* **2015**, *186*, 654–663. [[CrossRef](#)]
37. Dietz, H.; Radwan, M.; Döring, H.; Wiesener, K. On the hydrogen balance in sealed lead/acid batteries and its effect on battery performance. *J. Power Sources* **1993**, *42*, 89–101. [[CrossRef](#)]
38. Bullock, K.R. Carbon reactions and effects on valve-regulated lead-acid (VRLA) battery cycle life in high-rate, partial state-of-charge cycling. *J. Power Sources* **2010**, *195*, 4513–4519. [[CrossRef](#)]
39. Calábek, M.; Micka, K.; Křivák, P.; Bača, P. Significance of carbon additive in negative lead-acid battery electrodes. *J. Power Sources* **2006**, *158*, 864–867. [[CrossRef](#)]
40. Moseley, P.T.; Rand, D.A.J.; Peters, K. Enhancing the performance of lead-acid batteries with carbon—In pursuit of an understanding. *J. Power Sources* **2015**, *295*, 268–274. [[CrossRef](#)]
41. Pavlov, D.; Rogachev, T.; Nikolov, P.; Petkova, G. Mechanism of action of electrochemically active carbons on the processes that take place at the negative plates of lead-acid batteries. *J. Power Source* **2009**, *191*, 58–75. [[CrossRef](#)]

